Photodissociation of HBr on the surface of Ar_n clusters at 193 nm

Michal Fárník,* N. Hendrik Nahler,† and Udo Buck‡

Max-Planck-Institut für Dynamik und Selbstorganisation,

Bunsenstrasse 10, 37073 Göttingen, Germany

Petr Slavíček§ and Pavel Jungwirth

Institute of Organic Chemistry and Biochemistry,

Academy of Science of the Czech Republic,

and Center for Biomolecules and Complex Molecular Systems,

Flemingovo nam. 2, 16610 Prague 6, Czech Republic

Abstract

Photodissociation experiments are carried out for single HBr molecules absorbed on the surface of large Ar_n clusters with the average size of $\langle n \rangle = 159$ at the dissociation wavelength of 193 nm. The kinetic energy of the H atom fragments is measured exhibiting peaks at zero and two energies which mark completely caged and unperturbed fragments going into the two spin orbit channels of Br, respectively. The results are compared with Molecular Dynamics simulations which account for the quantum librational delocalization of the H atom in the HBr molecule and the substitutional surface position of the molecule at 27 K. The latter result is obtained from a trajectory study of the pick-up process under realistic conditions. Both channels are populated by mainly perpendicular transitions in agreement with the results for the bare molecule. The high intensity close to the energy of the excited Br* state mainly originates from slowed down dissociation products from the ground state. Calculations based on these realistic initial state conditions give also good agreement with the experimental results for the dissociation wavelength of 243 nm.

*Present address:J. Heyrovsky Institute of Physical Chemistry, Prague 8, Czech Republic

†Present address:University of Bristol, School of Chemistry, Bristol BS8 1TS, UK

‡Electronic address: ubuck@gwdg.de

§Present address:Department of Chemistry, University of Illinois, Urbana IL 61801, USA

I. INTRODUCTION

The photodissociation of molecules in different cluster environments has attracted considerable interest in recent years. Because of their finite size, the theoretical treatment is simplified and a direct comparison with experiments is greatly facilitated [1, 2]. Hydrogen halide molecules solvated in different rare gas clusters have served as prototype systems for such investigations using various theoretical approaches [3–19]. The reason is the very rich coupling of the different electronically excited states which lead asymptotically to the excited and ground spin-orbit states of the halogen fragment. Depending on the influence of this coupling, the behaviour changes significantly when going from HCl to HI [20–22]. While for HCl, the ground and excited state products are only reached by perpendicular transitions, HI exhibits a strict separation with a parallel transition to the excited and perpendicular transitions to the ground state products. The HBr molecule is an intermediate case which behaves like HCl when dissociated at 193 nm, and like HI when dissociated at 243 nm [23]. The results of the calculations demonstrate a strong size dependence when the molecule is placed inside the rare gas cage. After the closing of three shells, the probability of cage exit events goes to zero [13]. When the hydrogen halide molecule is placed in the outer shell of the rare gas cluster, the exit probability depends sensitively on the special surface site and on the librational motion of the molecule [9, 12, 13]. On the experimental side, the kinetic energy distribution of the dissociation products is a direct probe of the cage exit probability and the cage effect exhibiting fast or zero velocity of the fragments, respectively. For hydrogen halides, either small systems [24–26] or neat clusters have been studied [23, 27]. We tried to solve this problem systematically by investigating HBr, HI, and HCl molecules and their complexes in different rare gas clusters. The pick-up technique was used for placing the molecules on the surface and the coexpansion to embed them into the interior of the cluster [12, 13, 28–33]. For the system HBr-Ar$_n$, this led to the first direct comparison of measured and calculated kinetic energy distributions of the outgoing H atom upon photodissociation at 243 nm [13, 30]. While the results for the embedded case were in nice agreement, the surface case turned out to be more complicated. Better agreement of the calculation for $n = 146$ with the measured results for the averaged size of $\langle n \rangle = 139$ could only be obtained by adding to the results of the surface position also that of the position in the second shell. This, however, has been proved questionable in the meantime,

since new calculation of the landing process for the smaller HCl [33] and the larger HI [32] molecule on Ar_n clusters in this size range demonstrated that mainly the surface position is occupied. Here the realistic size parameters of the Ar-Ar interaction of the best-fit potential have been used [34]. The reason for the less good agreement of the calculated kinetic energy distribution of the H atoms from the photodissociation out of a surface position might be the sampling of the initial wavefunction where the coupling between the HBr vibration and the hydrogen librational motion is neglected. In the tail of the HBr absorption spectrum at 243 nm, this coupling starts to play a role. At the maximum of the Franck-Condon overlap at 193 nm, however, the theoretical treatment should work well. Therefore, we present here new data on the photodissociation of HBr-Ar_n for the cluster size of $\langle n \rangle = 159$ at 193 nm. In addition, we measure the dependence on the polarization angle which gives information on the type of the transition moment and the potential curves involved. On the theoretical side we will present new calculations of the photodissociation process using a better approach for the calculation of the initial state which takes into account the finite cluster temperature. This information is obtained from the simulation of the pick-up process using Molecular Dynamics and the correct Ar-Ar interaction potential.

II. EXPERIMENT

In these experiments the HBr doped argon clusters are generated in a molecular beam apparatus shown schematically in Fig. 1 [12, 33, 35, 36]. The HBr molecules are photodissociated with a UV light pulse of an excimer laser at 193 nm wavelength, and the H atom fragments are ionized via a 2+1 REMPI (resonance enhanced multi-photon ionization) scheme at 243 nm derived from another pulsed laser system. The ions are detected energy-sensitively in a Wiley-McLaren time-of-flight mass spectrometer (WM-TOFMS) operating in the so called low-field mode.

To prepare the HBr molecules in the surface region of the Ar cluster, the cluster beam is first produced by a supersonic expansion of neat Ar through a nozzle with conical shape with a diameter of 60 μm, an opening angle of 25° and a length of 2 mm at an expansion temperature of 221 K and pressure of 5 bar. The data are listed in Tab. I. The average cluster size of the Ar_n host clusters at these conditions is $\langle n \rangle = 159$, according to the relation provided by Hagena [37]. Between the second and third chamber, which are both

differentially pumped, the cluster beam passes through a scattering cell filled with HBr molecules at a partial pressure of $3 \cdot 10^{-2}$ mbar. In the resulting pick-up process under these conditions, it is most probable that only one HBr molecule is adsorbed by the Ar_n cluster [12]. In the course of this experiment the pick-up cell pressure was also varied up to $10 \cdot 10^{-2}$ mbar with very similar results as obtained for $3 \cdot 10^{-2}$ mbar. We should, however, note that in this case aside from the monomer also dimers might be present [12]

Following mixed cluster preparation the cluster beam enters the chamber containing the two-stage Wiley-McLaren type time-of-flight mass spectrometer (WM-TOFMS) [38]. To suppress the H atom background from hydrocarbons, the WM-TOFMS is surrounded by a copper shield mounted on a high-pressure helium compressor which results in a vacuum pressure of better than $2 \cdot 10^{-9}$ mbar. The cluster beam and the WM-TOFMS collection axis are oriented perpendicular to each other. The HBr molecules attached to the rare gas clusters are dissociated by a laser beam of 193 nm wavelength derived from an ArF/F_2-Excimer laser (Lambda Physics: LFP 202). The emitted light was polarized using a thin film polarizer (TFP), and sent into the detector chamber perpendicularly to both, the cluster beam and the WMTOF axis (see Fig. 1). The rotation of TFP about the laser beam axis allowed to change the laser light polarization from 0° to 90° polarization angle with respect to the WMTOF axis. The laser beam is focused by a 366 mm LiF lens onto a spot size of $\omega_0 \approx 10$ μm (Gaussian beam waist), in the intersection point of the cluster beam and the WMTOF axis. This yielded an intensity of $8{\cdot}10^{10}$ Wcm^{-2} at a typical laser energy of 4.9 mJ over 20 ns pulse length.

After the dissociation the H fragment ionization proceeded with a 243.06 nm laser beam generated by mixing the fundamental of a Nd:YAG laser (Quanta Ray GCR-5) with the frequency doubled output of a dye laser (LAS, LDL 20505) operated at 630.3 nm, and pumped by the second harmonic of the Nd:YAG laser. The laser pulses were repeated at a frequency of 10 Hz with a pulse length of 5 ns. The laser beam was focused into the detector chamber by a 400 mm quartz lens onto a spot of $\omega_0 \approx 14$ μm radius. The ionization laser beam was introduced into the detector chamber at 162.5° to the dissociation beam, in the plane of the cluster beam and the dissociation laser beam (see Fig. 1). The laser intensity at the focal spot was $2.2{\cdot}10^{11}$ Wcm^{-2} at a typical laser energy of 1.8 mJ. The polarization of the linearly polarized laser light was parallel (0° polarization angle) with respect to the WMTOF axis.

The time synchronization of the two laser beams was achieved by triggering the excimer laser by the Nd:YAG laser pulses via a pulse delay generator. The REMPI laser was slightly time-delayed by 5 to 10 μs with respect to the dissociation laser so that its shorter laser pulse length fitted completely into the longer laser pulse of dissociation laser. In this experiment the dissociation process is saturated so that the REMPI laser almost does not give any contribution to the HBr photolysis. The spatial overlap of the two laser beams focused to approximately $\sim$10 μm with the intersection point of the cluster beam and the WMTOF axis was adjusted with the intensity and symmetric shape of the H^+ time of flight distribution.

After the molecular photodissociation and successive ionization the ions are extracted by a small electric field of $\sim$9 V/cm into the WM-TOFMS. This operation in the above mentioned low-field mode causes a splitting of the peaks originating from ions which are directly ejected toward the detector and those with an initial velocity in the opposite direction; then the latter ions are decelerated in the extraction field and their velocities are reversed. In this way we are able to detect slow fragments, even those with initially zero kinetic energy, which give rise to a signal between the peaks of the fast ions. An example of a TOF spectrum is shown in Fig. 2. The intensity displays three peaks. The fastest and slowest ones are those which correspond to unperturbed cage exit events in the ground state of Br. The one in the middle refers to H atoms with zero kinetic energy.

To derive the key value, the kinetic energy distribution (KED) of the H atoms, from the TOF spectra we carry out a complete simulation of the particle trajectories taking into account the photodissociation process with its angular distribution, the velocity of the cluster beam, the finite interaction volume, the detector dimensions, the different electric deflection fields, and the electronic response function of the detector (MCP) [12, 23].

Crucial parameters in the KED transformation are the electrode voltages of the ion optics and the starting point of the ion trajectories defined by the interaction point of the REMPI laser with the molecular beam. The electrode voltages measured with the ion optics power supply exhibit an inaccuracy of up to 5%. This is partly due to an instrument error but also influenced by changes of the electrode charges, stray fields and further field inhomogeneities. The ion time-of-flights can be shifted by up to 40 ns with a change in the turn-around time of about 4 ns. Additional shifts of the time-of-flight spectra in the order of a few ns can be caused by an off-center photo-ionization. Both these errors have to be corrected in the TOF to KED transformation procedure. The three parameters to be adjusted in the fitting

procedure are as follows: extraction voltage, acceleration voltage (inaccurate fields) and starting point of the ions between the first two electrodes on the axis towards the detector (off-center photo-ionization). Each time-of-flight spectrum contains three pronounced well-defined features which we use to determine the set of parameters to a high precision before we proceed with the transformation. These peaks were already discussed in connection with Fig. 2.

The program to transform TOF to KED distributions [12] is based on the MC simulation program calculating mono-energetic TOF spectra [23]. Mono-energetic TOF spectra at zero kinetic energy and the highest available energy are calculated for a set of voltages and a start position of the ions. Comparison of the simulated spectra with the measured TOF spectrum guides the iterative process to determine the final parameter set for the electrode voltages and the starting position of the ions. With this set of parameters the TOF to KED transformation is performed.

The different contributions which can be derived from the measured kinetic energy of the H atom, E_{kin}(H), are best discussed in terms of the energy balance of the photodissociation

$$h\nu + E_{int}(\mathrm{HBr}) = D_0 + E_{int}(\mathrm{Br}) + E_{kin}(\mathrm{Br}) + E_{kin}(\mathrm{H}) + E_{clu} \qquad (1)$$

where the laser excitation energy $h\nu$ and the dissociation energy D_0 of HBr (3.745 eV) [39] are known, and E_{kin}(H) is measured. The kinetic energy of the Br fragment is known from conservation of momentum. The excitation of the upper spin-orbit state (Br*, 0.457 eV) of the Br product channel is allowed for by the term E_{int}(Br) and is measured as energy loss of the H atom. The influence of the cluster is expressed by the continuous energy loss E_{clu} of the H atoms caused by collisions and capturing processes with the Ar cage. This leads to delayed exit or perfect caging, depending on the position of the HBr molecule in the cluster environment and the initial direction of the H atom recoil. The HBr molecules are mainly prepared in their ground rotational and vibrational state in the pick-up process ($E_{int}(\mathrm{HBr}) = 0$).

III. EXPERIMENTAL RESULTS

In our experiments the polarization of the dissociating laser at 193 nm was changed. The results of the kinetic energy distributions of the H-atom, obtained for the polarization

angles 0° and 90° are given in Fig. 3. The data were obtained for 2.5 mJ/pulse of the REMPI laser, 3.5 - 4.7 mJ/pulse of the dissociation laser, and for a cell pressure of $10.0 \cdot 10^{-2}$ mbar. The spectra are dominated by large caging probabilities at zero kinetic energies which do not depend on the polarization. But also the other parts of the two spectra look remarkably similar. The main difference occurs at the position of the direct cage exit to the ground state at 2.68 eV. Here the measurement at 90° exhibits a pronounced shoulder which is not present in the measurement at 0° polarization. Surprisingly about the same intensity is observed for both polarizations at the energy of the excited spin orbit state Br* at 2.22 eV. This could be an indication that the intensity close to the excited state at 2.2 eV does not originate from direct cage exit processes but are caused by slowed down H atoms starting from the ground state. When we evaluate these data in terms of the known angular dependence $I(\theta) \approx \sigma(1 + \beta\ P_2(\cos\theta))$, we get for the β parameter of the excited state $\beta^* = -0.31 \pm 0.2$, and for the ground state $\beta = -0.95 \pm 0.2$. The branching fraction for the excited state is $\Gamma^* = \sigma^*/(\sigma + \sigma^*) = 0.71 \pm 0.14$. Thus both states are mainly populated by a perpendicular transition, but the intensity close to the excited state exit is much larger than that of the ground state. Before we start to draw conclusions out of these experimental results, we should look for a further experimental indication that the peak at 2.2 eV is independent of the polarization angle. In order to check this behaviour, we have repeated these measurements under slightly different conditions (cell pressure $3 \cdot 10^{-2}$ mbar; 3.2 mJ/pulse for the REMPI and 4.8 - 4.9 mJ/pulse for the dissociation laser) but adding the polarization angle 54.7° which is independent of the angular distribution. In addition, the lower cell pressure guarantees that only HBr molecules are captured and dissociated. The results are displayed in Fig. 4. In general, the direct cage exit probabilities are smaller than those of Fig. 3. This is a clear indication that the contributions of $(HBr)_2$ dimers lead to larger cage exit probabilities. For the polarization angles 0° and 90° similar features are observed with equal intensities for both states at 90° polarization. For the polarization angle of 54.7° a peak at the excited spin-orbit state and a shoulder with smaller intensity at the position of the ground state is found. Thus we have the clear result that around 2.2 eV the intensity is nearly independent of the polarization angle. When we evaluate these experimental data, we get for the β parameter of the excited state $\beta^* \approx -0.56 \pm 0.2$, and for the ground state $\beta \approx -0.85 \pm 0.2$. First, they agree within the error bars with those obtained in Fig. 3. Secondly, these values are not far away from the results of the bare molecule HBr

dissociated at 193 nm, for which $\beta^* = 0.0 \pm 0.1$ and $\beta = -0.9 \pm 0.1$ were obtained [23]. The latter values have been confirmed by a recent study of the photofragment alignment of HBr dissociated at 193 nm which results in $\beta^* = -0.2 \pm 0.1$ and $\beta = -0.88 \pm 0.1$ [40, 41]. Thus the excitations are dominated by perpendicular transitions (0.85) with a little bit of an admixture of a parallel transition (0.15). If we continue this analysis and derive the branching fraction for the excited state, we get in the present cluster case about $\Gamma^* = 0.68 \pm 0.05$, while for the bare molecule $\Gamma^* = 0.15$ was observed. Apparently, we have the result that the cluster environment enforces the population close to the excited spin-orbit channel but keeping the preferential excitation mechanism by a perpendicular transition for both channels. To learn something about the origin of this behaviour, we have to compare these data with calculations.

IV. SIMULATION OF THE EXPERIMENT

Simulation of large cryogenic HBr-Ar_n clusters created in a pick-up procedure represents a complex issue due to the large number of particles involved and the possibly strong quantum character of the system under experimental conditions. We have adopted here an approach similar to our previous studies [32]. The simulation protocol is based on the following assumptions: (i) the motion of the heavy atoms (argon and bromine) can be reasonably described by classical mechanics, (ii) the vibrational, rotational (librational), and translational motions of the HBr guest molecule can be adiabatically separated in the electronically ground state of the cluster, and (iii) the dynamics upon the photoexcitation is essentially a classical one.

The simulation follows the experimental procedures in a straightforward way. We first calculate the characteristics of the experimentally prepared clusters, i.e. we calculate the distribution of the heavy atoms (position of HBr molecule within the argon cluster geometries) following the pick-up process. We then calculate the librational wavefunction for a given cage geometry. In a third step, we perform the quasiclassical molecular dynamics on the excited state surfaces.

For comparison, we have also assumed clusters at T=0 K. In this case, the way we simulate these clusters is a bit different than what we do when simulating the experimental situation with the temperature of approximately 27 K. While this study concerns mostly the

photodissociation with a 193 nm laser pulse, we also make comparison with experimental and previous theoretical results obtained at 243 nm wavelength. Here again some minor changes in the theoretical treatment had to be assumed.

A. Pick-up simulations

To obtain the HBr distribution, we have directly calculated the outcome of the pick-up process rather than calculating the thermodynamical distributions. Argon clusters at low temperatures are of solid character and thus highly non-ergodic. The Molecular Dynamics method has been shown as a suitable tool for simulating the pick-up process [42]. The Lennard-Jones (LJ) potential has been used both for the description of argon-argon and argon-HBr interactions. The HBr molecule has been represented as a united atom here, with the parameters ϵ=121 cm^{-1} and σ=3.55 Å. These parameters correspond to the HBr molecule in a state of a free rotor interacting with argon atom, i.e. we have averaged the three body potential of Hutson [43] over all possible HBr orientations. Such an approximation is partially justified, since the three body potential is not very anisotropic. Note also that the Lennard-Jones parameters for the argon-argon interaction have been obtained by fitting the correct pairwise potential of Aziz and Slaman [34] to the Lennard-Jones form. As we have shown in our previous study, the LJ parameters usually used and taken from simulations of the liquid and solid represent a considerable bias and can not be used for the cryogenic cluster simulations [32].

We have applied the Verlet algorithm with a timestep 10 fs to integrate Newton's equations of motion. The argon cluster has been prepared at the temperature of 27 K. The cluster has been equilibrated for 10 ns. After a random rotation of the cluster, the dopant is sent with a random impact parameter to the cluster. Impact velocities are sampled from the 300 K distribution of the HBr, and the cluster beam velocity was taken to be 450 ms^{-1}. Each pick-up simulation lasted 50 ns. Altogether, 500 trajectories have been collected. We have started with a 130-atom cluster. During the pick-up simulation, several argon atoms have evaporated.

Smaller argon clusters exhibit icosahedral symmetry with solvation layers gradually surrounding the central atom. This structure feature is not changed by cluster heating t0 27 K. Although the HBr projectile can initially change locally the geometry, finally the system

settles with a geometry close to the original one. Figure 5a shows the density of argon atoms and the HBr dopant. The HBr molecule does not penetrate the argon cluster. Instead, it stays half solvated in the outer solvation shell. This position also corresponds to the minimum energy configurations in HBr-Ar_n clusters. While the HBr attractive interaction with the argon atom is higher than the interaction between argon atoms, the molecule is also somewhat too large to fit into an inner substitutional position.

The HBr distribution in the argon cluster can also be characterized by the number of argon atoms interacting close to HBr molecule. This is demonstrated in Fig. 5b. The argon atom is assumed to be close if the argon-bromine distance is smaller than 4.3 Å. Here again we can see that the major part of the HBr population interacts with about six argon atoms, corresponding to the surface half-solvated state.

If we compare this result of the landing of HBr on Ar_n clusters with those obtained for HI [32] and HCl [33] under otherwise similar conditions for the thermal velocities and the argon interaction potentials, we observe a very similar result as for HI. The dopant molecule stays half-solvated in the outer surface shell. The HI-Ar attractive forces are a little bit higher but the size is larger than that for HBr-Ar so that about the same position results. This is different for HCl-Ar. Here, the smaller interaction and size lead to a better penetration into the surface and the HCl matches almost perfectly with the Ar position of the outer shell with a slight tendency to penetrate into the second shell. This results in practically no cage exit events for HCl and cluster sizes around $n = 140$ [33].

Note also that in the cluster prepared by the co-expansion technique the HBr dopant stays in the central position even though this is not a thermodynamically stable one [13]. This confirms the assumption that argon clusters remain solid under experimental conditions. The neon clusters, under similar conditions, are solid too, however, with a rather fluid surface layer [31]. This is not true for argon clusters since argon atoms are more strongly bound and heavier the neon. Therefore, they exhibit less quantum behaviour than neon clusters. The quantum correction for the argon atom distribution has actually been neglected, since its effect is rather small [32].

B. Photodissociation dynamics

The photon pumps into the system enough energy so that the subsequent dynamics can be reasonably described by within classical dynamics. However, the quantum character of the initial state has to be properly taken into account. Namely, the HBr librational orientation determines the outcome of the photodissociation experiment.

The way we obtain the initial heavy atom positions (and velocities) differs whether our system is assumed to be prepared at T=27 K or at the temperature of absolute zero. In the first case, we have sampled the initial positions of the heavy atoms from the classical MD simulations of the the pick-up process. In the latter case, we have used the minimum energy configuration of the HBr-Ar_{147} cluster with three filled icosahedral layers.

Once we have generated the set of initial cage geometries, we have calculated the hydrogen librational wavefunction by diagonalizing the Hamiltonian

$$\hat{H} = \frac{\hat{j}^2}{2\mu_2 r^2} + V(\Theta, \Phi, \{q_i\}) \tag{2}$$

in a basis set of spherical harmonics. Here, μ is the reduced mass of the HBr molecule and $V(\Theta, \Phi, \{q_i\})$ is the full potential energy surface of the system. Θ and Φ are angular coordinates corresponding to the HBr librational motion and $\{q_i\}$ is a set of heavy atom coordinates. Notice, that in this approach the HBr intermolecular distance is kept frozen. When simulating clusters at T=0 K, the vibrations of the argon cage have been taken into account with the harmonic approximation.

The sampling from the pick-up simulation followed by the librational wavefunction calculation contains certain inconsistencies. The HBr-Ar effective potential has been generated under the assumption that the HBr molecule is a free rotor. While this treatment does not considerably bias the HBr center of mass distribution, it can strongly influence the librational wavefunction (i.e., the orientation of the hydrogen inside or out of the cluster). To avoid unphysically close contacts of HBr and argon atoms, we have optimized the HBr position in a fixed argon cage. During this optimization, the lowest eigenvalue of the Hamiltonian of Eq. 2 is minimized. While we could in principle have used the lowest eigenvalue of the Hamiltonian of Eq. (2) as the effective potential energy surface for the pick-up simulation, this would be computationally prohibitive for the duration of the simulation. The minimum

energy structure at T=0 K is obtained in a similar way, but now all the heavy atoms are allowed to relax.

The initial wavefunction is mapped onto coordinate-momentum phase space via the Wigner transformation [44]. This transformation is performed for the librational wavefunction and also for the harmonic vibrational wavefunction of the cage in the case of the T=0 K simulation. The distance HBr is adjusted so that the energy condition of Eq. (1) is fulfilled. In the case of the HBr excitation by the 243 nm laser pulse, the excitation corresponds to the red tail of the HBr absorption spectrum. The HBr distance in this case is prolonged. Now the hydrogen can strongly interact with the argon cage. Thus, for certain librational angles the energy balance of Eq. (1) cannot be achieved for any HBr internuclear distance.

The potential energy surface of the HBr-Ar_n complex has been essentially constructed in a pairwise additive way. To describe the HBr photodissociation, we have adopted the two state model previously used by Huang and Guo [45]. The two states involved are the $^1\Pi_1$ and the $^3\Pi_{0+}$ state; the first one correlates asymptotically with the ground state Br, while the latter one corresponds to the excited spin orbit state of bromine (Br*). At the 193 nm excitation, the oscillatory strength is dominated by the $^1\Pi_1$ state. Thus at this excitation wavelength, there is only a negligible transition probability directly into the $^3\Pi_{0+}$ state. In the course of the photodissociation dynamics, the two curves cross and non-adiabatic events may occur. We accounted for these by the Landau-Zener model with parameters taken from Ref. [45]. For the photoexcitation by the 243 nm laser pulse, the parallel transition into the $^3\Pi_{0+}$ is actually responsible for the observed Br*/Br branching ratio rather than non-adiabatic events in the course of the dynamics. In the experiment, a polarized laser beam is used. As we have shown for the HI photodissociation [32], we may nevertheless observe a contribution from the parallel transition due to the hydrogen scattering from the argon cage. Since the branching fraction at 243 nm is only about 17 %, we decided to ignore the role of the parallel transition here. Notice that in our previous study [13] we have assumed that the scattering from the cage completely randomizes the hydrogen atoms before they leaves the cage. If this was completely true, then the experimentally observed KED spectrum would be the same as the one from the unpolarized experiment. The argon-argon interaction was described by a fitted Lennard-Jones potential (see the previous section), the argon-hydrogen potential was taken from Ref. [11], and the Br-Ar_n has been modelled using

the DIM approach as is described in Ref. [13].

The classical trajectories have been run for 3 ps, with a time step 0.0241 fs. Approximately 1000 trajectories have been collected for each excitation wavelength and temperature. This number of trajectories provides well converged results.

The simulated hydrogen kinetic energy distribution (KED) spectra for the two wavelengths and for simulations performed at two temperatures are shown in Fig. 6. The increasing temperature apparently increases the probability of the hydrogen exit from the cage. At the temperature T= 0 K, the HBr guest occupies the ideal substitutional position, while other less convenient sites starts to be populated when increasing the temperature. The difference is, however, not large. This is in accord with the pick-up simulations, showing that the substitutional position be dominantly populated even at the temperature T= 27 K. By decreasing the excitation wavelength, the hydrogen atom has initially a larger amount of excess energy available. Thus, the exit maximum shifts by 0.9 eV. The fraction of the trapped hydrogen atoms is smaller for 193 nm excitation than it was for 243 nm. The cage is, however, still able to slow down a significant fraction of the hydrogen atoms to zero velocity.

V. COMPARISON WITH EXPERIMENTAL RESULTS AND DISCUSSION

The analysis of the photodissociation of the bare HBr molecule at 193 nm clearly shows that the ground and the excited spin-orbit state of Br are mainly populated by a perpendicular transitions [23, 41]. In the latter case a small admixture of a parallel transitions is present. A general notion is accepted that after the excitation from the ground state to the $^1\Pi_1$ state the population of the excited state is obtained by non-adiabatic coupling to the $^3\Pi_{0+}$ state. This result does not change by placing the HBr molecule on the surface a large Ar_n cluster as was demonstrated in Sec. III. Therefore, it is reasonable to compare the experimental results of Fig. 4 at 54.7° polarization with the calculation of the photodissociation dynamics described in detail in Sec. IVb and exhibited in Fig. 6. We have chosen the measurement at 54.7° and not the one at 90° polarization, since in the present calculations the angular dependence is not specified as was done for HI-Ar_n [32]. The result of this comparison is displayed in Fig. 7. We have normalized the two curves to the integrated intensity. In this way we avoid problems with the different energy resolution of

experiment and calculations and with artificial spikes of the data evaluation procedure. The general agreement between experiment and theory is very good. The main features of the experiment, the peak at zero energy caused by caged H atoms and the broad peak close to the direct cage exit position between 2.2 and and 2.6 eV, are correctly reproduced by the calculations. This gives us confidence that our model, the simulation of the pick-up process at the realistic cluster temperature of 27 K and the use of this results as initial state in the subsequent photodissociation process, is reasonable. The same is valid for the further simplified two-state calculation using the Landau-Zehner model for the coupling to the excited state. It mainly includes the excitation to the $^1\Pi_1$ potential curve which, in turn, decays to the ground state. This model is in agreement with the experimental result of a mainly perpendicular transition which populates both states. We note that the calculation reasonably reproduces the correct intensities in the region of the cage exit events. This means that the intensity close to the position of the excited state at 2.2 eV and at smaller energies are mainly caused by slowed down H atoms and to a lesser extent by a direct excitation to the excited state. This plays a role here, since the higher kinetic energy available at 193 nm leads also to a more effective energy exchange when the H atom is originally flying into the direction of the cluster interior.

The higher cage exit probabilities which we have observed for the results of Fig. 3 are traced back to the presence of $(HBr)_2$ dimers in the surface. While in one of the HBr molecules the H atom points, like in the case of the monomer, towards the inside of the cluster, the other is situated perpendicular to it with the H atom pointing to the Br atom of the first molecule [29]. This position opens up a much higher possibility for cage exit events which also undergo energy loss processes. Aside from this, the results do not differ very much from the monomer case.

The good agreement of experiment and simulations at 193 nm encouraged us to re-analyze the experimental results at 243 nm [12] where we had problems with the interpretation [30]. This comparison is shown in Fig. 8. Here we compared the calculations with a measurement using unpolarized radiation. We get a nearly perfect agreement in the amplitudes of the cage exit at 1.3 eV and the caged events at 0.0 eV. There is a slight shift in the energy at the exit channel which might have its origin in the close interaction of the H atom with the Ar atoms as was mentioned in the theory section. The much better agreement in the amplitudes compared with the previous analysis can be traced back to the improved

theoretical treatment applied in this work . First, the higher temperature of 27 K instead of 0 K leads to a higher cage exit probability as is demonstrated in Fig. 6. In addition, also at 0 K this probability is larger than the one calculated previously, because of a different sampling procedure applied in the present calculation which takes into account all events.

In conclusion, the theoretical treatment presented here is able to reproduce the experiments of HBr molecules on the surface of large Ar_n clusters in the size range of $\langle n \rangle = 159$ for both wavelengths of 193 nm and 243 nm. We note that the physical mechanisms are partly different for the two wavelengths. At both wavelengths the excitation goes through a perpendicular transition into the ground spin-orbit state. At 243 nm in the tail of the Franck-Condon overlap this remains practically the only channel. At 193 nm in the middle of the Franck-Condon region the population of the excited state is larger than that of the ground state and cage exit is mainly caused by slowed down H atoms.

In contrast, the HCl molecules, photodissociated at 193 nm, do not show any cage exit events, since, in this case, the molecule fits better in a substitutional position of the Ar_n cluster so that in the investigated size range no H atom could leave the cluster [33]. The comparison with results for HI at 243 nm exhibits a similar behaviour concerning the population of the ground and the excited state [32]. They are equally populated, but in this case the final population of the ground state comes from a perpendicular transition and that of the excited state from a parallel transition. In addition, the intensities are mixed by scattering processes from the surrounding Ar atoms of the cluster.

Acknowledgments

This work was supported by the Deutsche Forschungsgemeinschaft in SFB 357. Support from the Czech Ministery of Education to the Center for Biomolecules and Complex Molecular Systems (Grant No. LC512) is gratefully acknowledged. Part of th ework in Prague was supportedvia the Research Project Z40550506.

[1] R. B. Gerber, A. B. McCoy, A. García-Vela, Ann. Rev. Phys. Chem. 45 (1994) 275.

[2] U. Buck, J. Phys. Chem. A 106 (2002) 10049.

[3] R. Alimi, R. B. Gerber, Phys. Rev. Lett. 64 (1990) 1453.

[4] A. García-Vela, R. B. Gerber, U. Buck, J. Phys. Chem. 98 (1994) 3518.

[5] T. Schröder, R. Schinke, S. Liu, Z. Bačić, J. W. Moskowitz, J. Chem. Phys. 103 (1995) 9228.

[6] E. Narevicius, D. Neuhauser, H. J. Korsch, N. Moiseyev, Chem. Phys. Lett. 276 (1997) 250.

[7] M. Niv, A. I. Krylov, R. B. Gerber, Faraday Discuss. Chem. Soc. 108 (1997) 243.

[8] A. García-Vela, J. Chem. Phys. 108 (1998) 5755.

[9] M. Y. Niv, A. I. Krylov, R. B. Gerber, U. Buck, J. Chem. Phys. 110 (1999) 11047.

[10] P. Žďánská, B. Schmidt, P. Jungwirth, J. Chem. Phys. 110 (1999) 6246.

[11] P. Žďánská, P. Slavíček, P. Jungwirth, J. Chem. Phys. 112 (2000) 10761.

[12] R. Baumfalk, N. H. Nahler, U. Buck, M. Y. Niv, R. B. Gerber, J. Chem. Phys. 113 (2000) 329.

[13] P. Slavíček, P. Žďánská, P. Jungwirth, R. Baumfalk, U. Buck, J. Phys. Chem. 104 (2000) 7793.

[14] P. Slavíček, M. Roeselová, P. Jungwirth, B. Schmidt, J. Chem. Phys. 114 (2001) 1539.

[15] M. Monnerville, B. Pouilly, Chem. Phys. Lett. 294 (1998) 473.

[16] B. Schmidt, Chem. Phys. Lett. 301 (1999) 207.

[17] J. Trin, M. Monnerville, B. Pouilly, H.-D. Meyer, J. Chem. Phys. 118 (2003) 600.

[18] R. Prosmiti, A. Garcia-Vela, J. Chem. Phys. 118 (2003) 8268.

[19] S. López-López, A. Garcia-Vela, J. Chem. Phys. 120 (2004) 660.

[20] H. M. Lambert, P. J. Dagdigian, M. H. Alexander, J. Chem. Phys. 108 (1998) 4460.

[21] G. Peoux, M. Monnerville, T. Duhoo, B. Pouilly, J. Chem. Phys. 107 (1997) 70.

[22] R. J. LeRoy, G. T. Kraemer, S. Manzhos, J. Chem. Phys. 117 (2002) 9353.

[23] R. Baumfalk, U. Buck, C. Frischkorn, N. H. Nahler, L. Hüwel, J. Chem. Phys. 111 (1999) 2595.

[24] J. Segall, Y. Wen, R. Singer, C. Wittig, A. García-Vela, R. B. Gerber, Chem. Phys. Lett. 207 (1993) 504.

[25] J. Zhang, M. Dulligan, J. Segall, Y. Wen, C. Wittig, J. Phys. Chem. 99 (1995) 13680.

[26] K. Liu, A. Kolessov, J. W. Partin, I. Brezel, C. Wittig, Chem. Phys. Lett. 299 (1999) 374.

[27] M. A. Young, J. Chem. Phys. 102 (1995) 7925.

[28] R. Baumfalk, N. H. Nahler, U. Buck, Faraday Disscus. 118 (2001) 247.

[29] R. Baumfalk, N. H. Nahler, U. Buck, Phys. Chem. Chem. Phys. 3 (2001) 2372.

[30] N. H. Nahler, R. Baumfalk, U. Buck, H. Vach, P. Slavíček, P. Jungwirth, Phys. Chem. Chem. Phys. 5 (2003) 3394.

[31] P. Slavíček, P. Jungwirth, M. Lewerenz, N. H. Nahler, M. Fárník, U. Buck, J. Phys. Chem. A 107 (2003) 7743.

[32] P. Slavíček, P. Jungwirth, M. Lewerenz, N. H. Nahler, M. Fárník, U. Buck, J. Chem. Phys. 120 (2004) 4498.

[33] N. H. Nahler, M. Fárník, U. Buck, H. Vach, R. B. Gerber, J. Chem. Phys. 121 (2004) 1293.

[34] R. A. Aziz, M. J. Slaman, Mol. Phys. 58 (1986) 679.

[35] U. Buck, R. Galonska, H. J. Kim, P. Lohbrandt, C. Lauenstein, M. Schmidt, in: R. Campargue (Ed.), Atomic and Molecular Beams. The State of the Art 2000, Springer, Berlin, 2001, p. 623.

[36] R. Baumfalk, U. Buck, C. Frischkorn, S. R. Gandhi, C. Lauenstein, Ber. Bunsenges. Phys. Chem. 101 (1997) 606.

[37] O. F. Hagena, Surf. Sci. 106 (1981) 101.

[38] W. C. Wiley, I. H. McLaren, Rev. Sci. Instrum. 26 (1955) 1150.

[39] P. M. Regan, S. R. Langford, A. J. Orr-Ewing, M. N. R. Ashfold, J. Chem. Phys. 110 (1999) 281.

[40] T. P. Rakitsis, P. C. Samartzis, R. L. Toomes, L. Tsigaridas, M. Coriou, D. Chestakov, A. T. J. B. Eppink, D. H. Parker, T. N. Kitsopoulos, Chem. Phys. Lett. 364 (2002) 115.

[41] T. P. Rakitsis, P. C. Samartzis, R. L. Toomes, T. N. Kitsopoulos, J. Chem. Phys. 121 (2004) 7222.

[42] H. Vach, J. Chem. Phys. 111 (1999) 3536.

[43] J. M. Hutson, J. Chem. Phys. 91 (1989) 4455.

[44] M. Hillery, R. F. O'Connel, M. O. Scully, E. P. Wigner, Phys. Rep. 106 (1984) 121.

[45] Z. Huang, H. Guo, J. Chem. Phys. 96 (1992) 8564.

TABLE I: Beam data

diameter of conical nozzle (μm)	60
expansion pressure (bar)	5.0
nozzle temperature (K)	221
pick-up pressure of HBr (mbar)	$3{\cdot}10^{-2}$
average cluster size $\bar{n}$	159

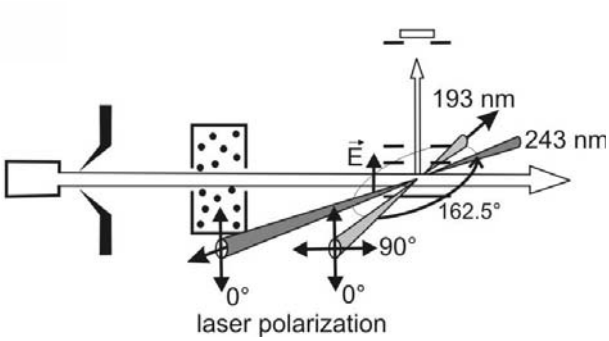

FIG. 1: Schematic view of the experimental apparatus: 193 nm dissociation and 243 nm ionization laser beams.

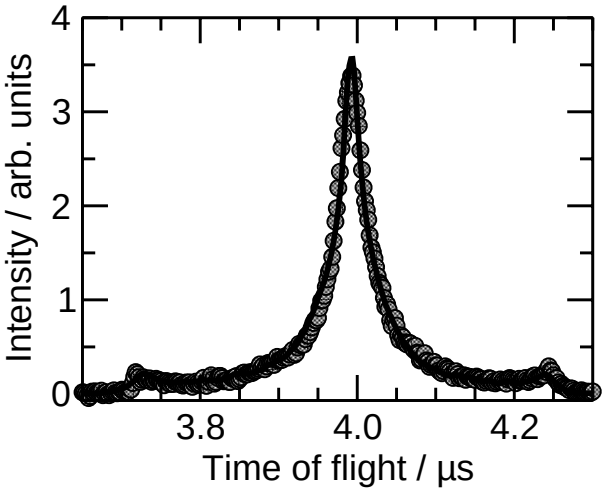

FIG. 2: Measured time-of-flight distributions for HBr-Ar_{159}.

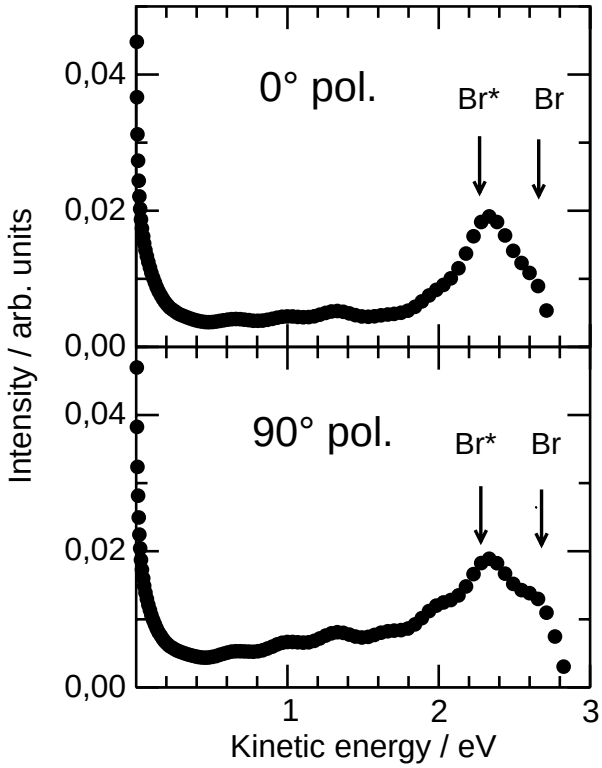

FIG. 3: Measured kinetic energy distributions for HBr-Ar_{159} for different polarization angles of the dissociating laser at 193 nm. The cell pressure is $1 \cdot 10^{-1}$ mbar.

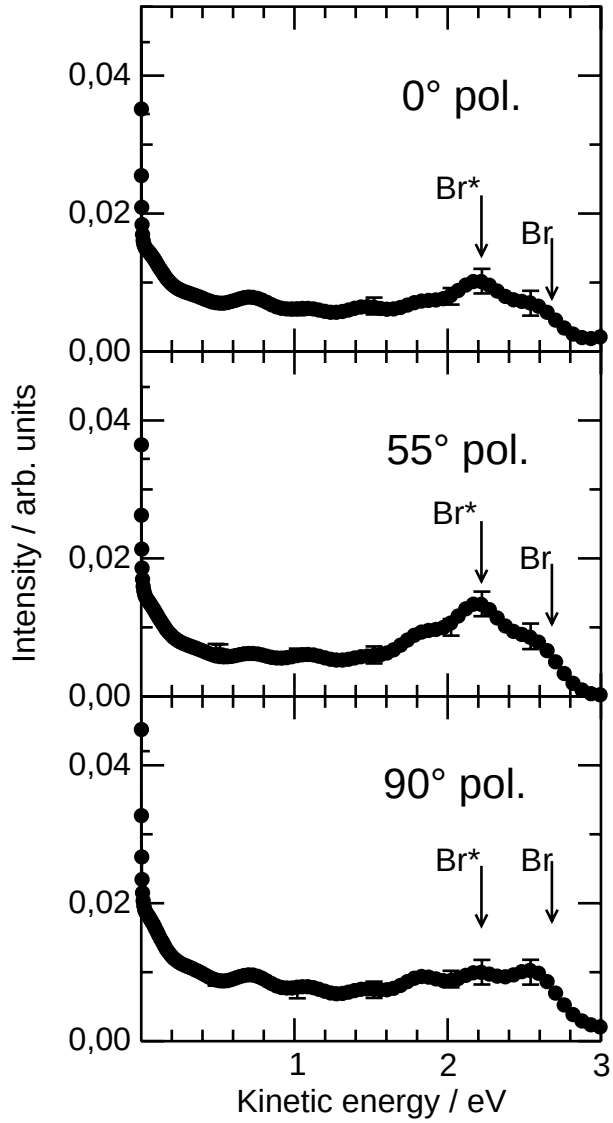

FIG. 4: Measured kinetic energy distributions for HBr-Ar_{159} for different polarization angles of the radiation of the dissociating laser at 193 nm. The cell pressure is $3{\cdot}10^{-2}$ mbar.

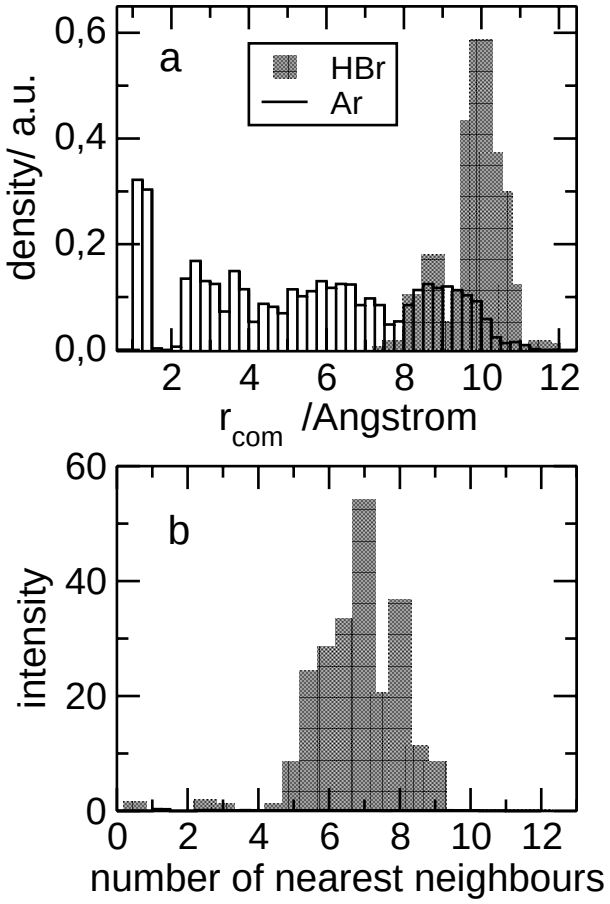

FIG. 5: a) Radially resolved species densities for Ar atoms and HBr guest molecules in Ar_{130} host clusters as a result of a pickup process under quasi-experimental conditions. The black lines give the density of the Ar atoms and the grey bars that of the HBr dopants. b) The distribution of ther number of nearest argon neighbours around the HBr molecule.

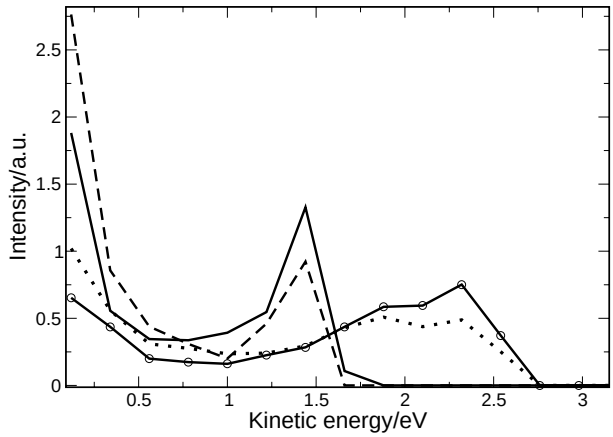

FIG. 6: Calculated kinetic energy distributions of HBr-Ar$_n$ with $n = 146$ and HBr in the outer shell for two different dissociation wavelengths and two different temperatures. Solid: 243 nm, 27 K; dashed: 243 nm, 0 K; solid with points: 193 nm, 27 K; dotted: 193 nm, 0 K.

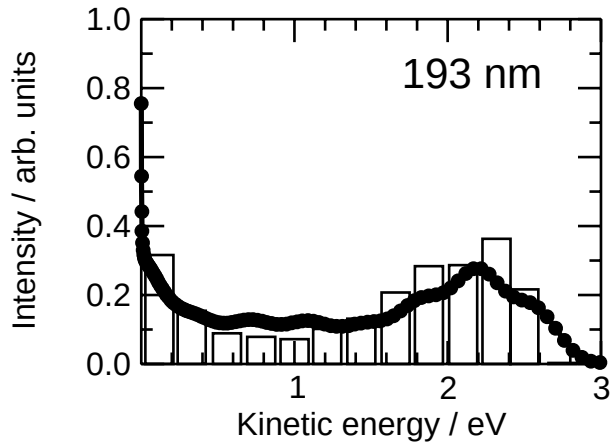

FIG. 7: Comparison of measured (points) kinetic energy distributions of HBr-Ar$_n$ for $\langle n \rangle = 159$ at 193 nm and 54.7° polarization angle with calculations (bars). The calculations are carried out as described in Sec.IV for n=146, 193 nm and 27 K (see also Fig. 6).

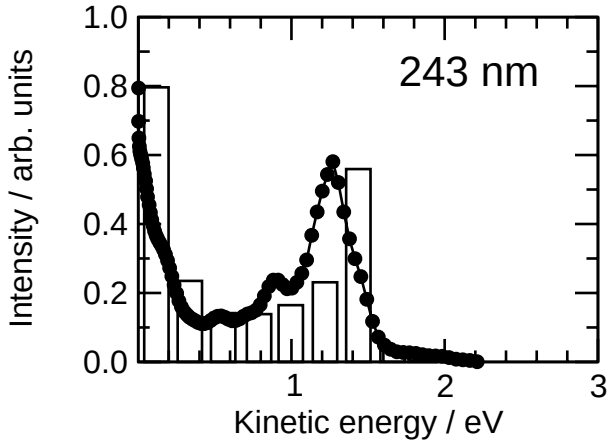

FIG. 8: Comparison of measured (points) and calculated (bars) kinetic energy distributions of HBr-Ar$_n$ for n=146 and $\langle n \rangle = 159$ at 243 nm.